Available online at www.sciencedirect.com
ScienceDirect
International Journal of Mass Spectrometry 268 (2007) 83–92
International Journal of Mass Spectrometry
www.elsevier.com/locate/ijms

High performance MALDI-TOF mass spectrometry for proteomics

Marvin Vestal, Kevin Hayden

Virgin Instruments Corp., Sudbury, MA 01701, USA

Received 12 March 2007; received in revised form 18 June 2007; accepted 25 June 2007
Available online 30 June 2007

Abstract

Theoretical techniques for optimizing the resolving power of TOF MS systems are presented, particularly for applications employing MALDI. These techniques are employed to design both a linear and a reflecting analyzer. Preliminary results on the performance of these instruments on proteins and peptides are presented, and compared with the theoretical predictions. Discrepancies between theory and experiment are analyzed, and further improvements are proposed.

Keywords: MALDI-TOF; Resolving power; Proteomics

1. Introduction

The invention of matrix-assisted laser desorption-ionization (MALDI) by Karas and Hillenkamp [1] has sparked a revival of interest in time-of-flight mass spectrometry (TOF). MALDI mass spectrometers are commercially available from a number of vendors and it is now an established technique for analyzing a variety of nonvolatile molecules including proteins, peptides, oligonucleotides, lipids, glycans, and other molecules of biological importance. While this technology has been applied to many applications, electrospray MS and MS–MS, particularly with on-line coupling to capillary HPLC separation, has achieved much wider acceptance. More rapid acceptance of electrospray following the invention by Fenn et al. [2] is at least partly due to compatibility with widely used analyzers such as quadrupoles and ion traps, while TOF analyzers were not widely available prior to the development of MALDI. While enormous progress has been made in the development of higher performance mass analyzers for both electrospray and MALDI in the years following introduction of these new ionization techniques, applications for MALDI have not developed as rapidly as those for electrospray.

Widespread acceptance of MALDI may be limited by many factors including cost and complexity of the instruments, relatively poor reliability, and insufficient performance in terms of speed, sensitivity, resolution, and mass accuracy. Different types of TOF analyzers are required depending on the properties of the molecules to be analyzed. For example, a simple linear analyzer is preferred for analyzing high mass ions such as intact proteins, oligonucleotides, and large glycans, while a reflecting analyzer is required to achieve sufficient resolving power and mass accuracy for analyzing peptides and small molecules. Determination of molecular structure by MS–MS techniques requires yet another analyzer. In some commercial instruments all of these types of analyzers are combined in a single instrument. This has the benefit of reducing the cost somewhat relative to three separate instruments, but the downside is a substantial increase in complexity, reduction in reliability, and compromises are required that make the performance of all of the analyzers less than optimal.

In earlier work a comprehensive theoretical model of the various components of a TOF analyzer was developed with a view toward optimizing performance of a complete system for particular applications [3]. The first application of this theoretical approach was the design of a family of MALDI-TOF instruments employing delayed extraction [4]. Recently the theoretical treatment has been recast in a form that allows the optimum design of an analyzer to be determined within external restrictions such as overall size and maximum accelerating voltage, and as restricted by specified initial conditions such as the initial velocity spread and initial uncertainty in ion position. Advances in related technology such as high-speed lasers, faster digitizers with on-board averaging, fast high-voltage pulse generators,

E-mail address: marvin.vestal@virgininstruments.com (M. Vestal).

1387-3806/$ – see front matter © 2007 Elsevier B.V. All rights reserved.
doi:10.1016/j.ijms.2007.06.021

and computer-controlled digital delay generators have made very high-performance TOF analyzers feasible. These technical advances combined with theoretical predictions provide new designs for MALDI-TOF MS systems that out-perform earlier instruments.

In this paper theoretical techniques for optimizing the resolving power of TOF MS systems are presented, particularly for applications employing MALDI. These techniques are employed to design both a linear and a reflecting analyzer. Preliminary results on the performance of these instruments on proteins and peptides are presented, and compared with the theoretical predictions. Discrepancies between and theory and experiment are analyzed, and further improvements are proposed.

2. Theoretical background

2.1. Ion source

A potential diagram for a generic two-stage ion source for TOF is illustrated in Fig. 1. The time focusing properties of this ion source were fully described in the pioneering paper by Wiley and McLaren [5].

The focal lengths for first order space and velocity focusing, respectively, are given by

$$D_s = 2d_0 y^{3/2}\left[1 - \frac{d_1/d_0}{y^{1/2}+y}\right] \quad (1)$$

$$D_v = D_s + \frac{(2d_0 y)^2}{v_n^* \Delta t} \quad (2)$$

where d_0 is the length of the first acceleration region, d_1 the length of the second acceleration region, Δt the time lag between ion production and application of the accelerating field, V the total acceleration potential, V_g the potential applied to the extraction grid, $y = V/(V - V_g)$, and v_n^* is the nominal final velocity of the ion of mass m^* focused at D_v. v_n^* is given by

$$v_n^* = C_1\left(\frac{V}{m^*}\right)^{1/2} \quad (3)$$

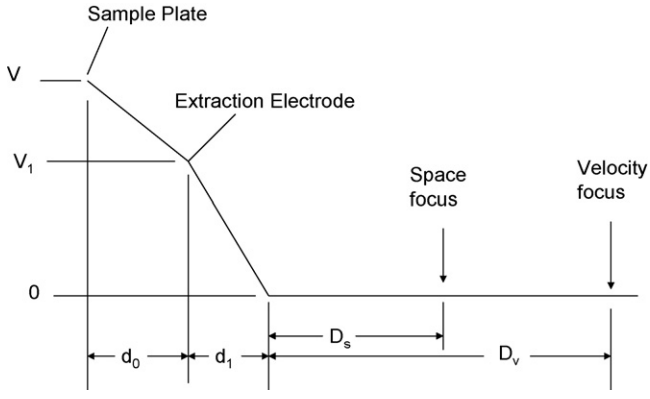

Fig. 1. Potential diagram for a two-stage pulsed time-of-flight ion source. The potential applied to the sample plate is pulsed from potential V_1 to V at a predetermined time Δt following production of a pulse of ions from the sample plate.

The numerical constant C_1 is given by

$$C_1 = \left(\frac{2z_0}{m_0}\right)^{1/2} = \left[\frac{2 \times 1.60219 \times 10^{-19}\,\mathrm{C}}{1.66056 \times 10^{-27}\,\mathrm{kg}}\right]^{1/2} = 1.38914 \times 10^4 \quad (4)$$

For V in V and m in Da (or m/z) the velocity of an ion is given by

$$v\,(\mathrm{m/s}) = C_1\left(\frac{V}{m}\right)^{1/2} \quad (5)$$

It is numerically more convenient in many cases to express distances in mm and times in ns. In these cases $C_1 = 1.38914 \times 10^{-2}$, and v is in units of mm/ns. The focal lengths of a single-field pulsed ion source with delayed extraction are also given by Eqs. (1) and (2) with $y = 1$ and $d_1 = 0$. The total effective flight distance D_e corresponds to the length of a field-free region for which the flight time is identical to that through the actual system.

The time-of-flight is measured relative to the time that the extraction pulse is applied to the source electrode. The extraction delay Δt is the time between application of the laser pulse to the source and the extraction pulse. The measured flight time is relatively insensitive to the magnitude of the extraction delay, but jitter between the laser pulse and the extraction pulse causes a corresponding error in the velocity focus. In cases where Δt is small, this can be a significant contribution to the peak width. This contribution due to jitter δ_j is given by

$$R_\Delta = 2\left(\frac{\delta_j}{\Delta t}\right)\left(\frac{\delta v_0}{v_n^*}\right)\frac{D_v - D_s}{D_e} = 2\left(\frac{\delta_j \delta v_0}{D_e}\right)\left(\frac{D_v - D_s}{2d_0 y}\right)^2 \quad (6)$$

and is independent of mass. δv_0 is the width of the initial velocity distribution.

Second order space focusing is not possible with a single-stage source, but as noted previously [3], simultaneous first and second order velocity focusing occurs at

$$D_{v2} = D_v = 6d_0 \quad (7)$$

with

$$\frac{d_0}{v_n^* \Delta t} = 1 \quad (8)$$

The relative contribution to peak width due to variation δx in the initial position of the ions is given by

$$R_{s1} = \frac{D_v - D_s}{D_e}\left(\frac{\delta x}{d_0 y}\right) \quad (9)$$

and D_e is the total effective flight length of the ions. With delayed extraction, the focal length of the source is mass dependent, and the contribution to peak width for ions other than the focused

mass is given by

$$R_m = R_{v1}\left[1 - \left(\frac{m}{m^*}\right)^{1/2}\right] \tag{10}$$

where the absolute value of the quantity in [ ] brackets is implied, and

$$R_{v1} = \left(\frac{4d_0 y}{D_e}\right)\left(\frac{\delta v_0}{v}\right) \tag{11}$$

and δv_0 is the width of the initial velocity distribution. With first order velocity focusing the contribution to relative peak width due to velocity spread is given by

$$R_{v2} = 2\left[\frac{2d_0 y}{D_v - D_s}\right]^2\left(\frac{\delta v_0}{v}\right)^2 \tag{12}$$

If $D_v = D_{v2}$ then the focus at D_v is independent of initial velocity to both first and second order, and the contribution to peak width at the focused mass due to the initial velocity distribution is given by

$$R_{v3} = 2\left[\frac{2d_0 y}{D_v - D_s}\right]^3\left(\frac{\delta v_0}{v}\right)^3 \tag{13}$$

The best resolving power is obtained by making D_e as large as possible within the overall geometric constraints imposed by the overall size of the instrument.

2.2. Ion reflector

A potential diagram for a reflecting analyzer with two-stage mirror [6] and single-stage source is shown in Fig. 2. The major advantage from adding a reflector is that it allows the effective length to be increased without increasing the other contributions to peak width so that optimal performance can be obtained with practical values of the parameters.

The first and second order focal lengths of the two-stage mirror are given by

$$D_{m1} = 4d_4 w^{3/2} + 4d_3\left[\frac{w}{w-1}\right][1 - w^{1/2}] \tag{14}$$

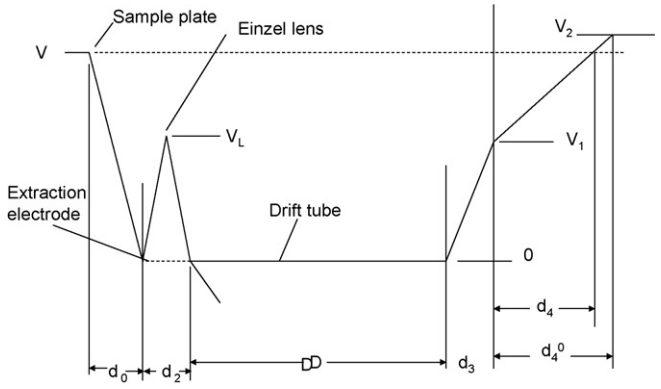

Fig. 2. Potential diagram for a reflecting TOF analyzer with single-stage ion source and two-stage ion mirror.

$$3D_{m2} = 4d_4 w^{5/2} + 4d_3\left[\frac{w}{w-1}\right][1 - w^{3/2}] \tag{15}$$

where d_3 is the length of the first region of the mirror, d_4 the distance than an ion with initial energy V penetrates into the second region of the mirror and $w = V/(V - V_1)$ is the ratio of the ion energy at the entrance to the mirror to that at the entrance to the second region with the intermediate electrode at potential V_1. The distance d_4 is related to the physical length of the second stage of the mirror d_4^0 by

$$d_4 = d_4^0\frac{V - V_1}{V_2 - V_1} \tag{16}$$

where V_2 is the potential applied to the back of the mirror.

The conditions for simultaneous first and second order focusing are derived by setting these focal distances equal, but these can be varied independently, for example by adjusting d_4 by changing V_2 according to Eq. (16). First and second order velocity focusing in a reflector requires satisfying the following equations:

$$\frac{4d_3}{D_m} = \frac{w-3}{w}, \qquad \frac{4d_4}{D_m} = w^{-3/2} + \left(\frac{4d_3}{D_m}\right)(w + w^{1/2}) \tag{17}$$

Thus, first and second order focusing can be achieved for any value of $w > 3$, and the corresponding distance ratios are uniquely determined by Eq. (17). The effective length of a two-stage mirror is given by

$$D_{em} = 4d_4 w^{1/2} + 4d_3\left[\frac{w}{w-1}\right][1 - w^{-1/2}] \tag{18}$$

An einzel lens is included in the analyzer depicted in Figs. 1 and 2 to focus the ions spatially at the detector. Such lenses have a negligible effect on time focusing, but do modify the effective flight distance. For a lens of total length d_2 biased at potential V_L the effective length of the lens is approximately

$$D_{eL} = 2d_2 Z\left[1 - (1 - Z^{-1})^{1/2}\right], \quad \text{where } Z = \frac{V}{V_L} \tag{19}$$

The effective length of the lens is included in the effective length of the field-free space between the exit from the source and the detector.

The dependence on the uncertainty in the time measurement δt is given by

$$R_t = \frac{2\delta t}{t} = \frac{2\delta t C_1}{D_e}\left(\frac{V}{m}\right)^{1/2} \tag{20}$$

where D_e is the total effective flight distance.

The dependence on trajectory error δL is given by

$$R_L = \frac{2\delta L}{D_e} \tag{21}$$

A major contribution to δL is often the entrance into the channel plates of the detector. If the channels have diameter d and

angle α relative to the beam, the mean value of δL is $d/2\sin\alpha$. Thus this contribution is

$$R_{\mathrm{L}} = \frac{d}{D_{\mathrm{e}} \sin \alpha} \tag{22}$$

Another important contribution to peak width due to trajectory error may be introduced by alignment between the ion reflector and the detector. If the angle between the plane of the detector and the effective plane of the reflector is β, then the contribution to peak width is given by

$$R_{\mathrm{Ld}} = \frac{2d_{\mathrm{d}} \sin \beta}{D_{\mathrm{e}}} \tag{23}$$

where d_{d} is the active diameter of the detector.

Noise and ripple on the high voltage supplies can also contribute to peak width. This term is given by

$$R_{\mathrm{V}} = \frac{\Delta V}{V} \tag{24}$$

where ΔV is the variation in V in the frequency range that effects the ion flight time.

It is obvious from these equations that increasing the effective length of the analyzer increases the resolving power, but some of the other effects are less obvious. The total contribution to peak width due to velocity spread is given by

$$R_{\mathrm{v}} = R_{\mathrm{m}} + \left(\frac{\Delta D_{12}}{D_{\mathrm{e}}}\right) R_{\mathrm{v2}} + \left[\frac{D_{\mathrm{e}} - \Delta D_{12}}{D_{\mathrm{e}}}\right] R_{\mathrm{v3}} \tag{25}$$

where ΔD_{12} is the absolute value of the difference between D_{v1} and D_{v2}. Assuming that each of the other contributions to peak width is independent, the overall resolving power is given by

$$R^{-1} = [R_{\mathrm{s1}}^2 + R_{\mathrm{v}}^2 + R_{\mathrm{t}}^2 + R_{\mathrm{L}}^2 + R_{\mathrm{V}}^2]^{-1/2} \tag{26}$$

2.3. Optimization of the linear analyzer

The potential diagram for a new linear TOF is shown in Fig. 3. While this design is superficially similar to previous linear analyzers, it has several unique features. First, the sample plate and extraction electrode are biased at a relatively low positive voltage (ca. 5–8 kV) and a pulsed positive of amplitude 5–2 kV is capacitively coupled to the source plate to produce a total source voltage of 10 kV. A first-field free region is located adjacent to the extraction electrode, and deflection electrodes for correcting for minor misalignments and for gating the ion beam to limit the mass range of transmitted ions are located in this field-free region. The ions are then further accelerated by an additional 30 kV, focused with an einzel lens employing a central electrode nominally at ground potential and travel through a second field-free drift tube maintained at a potential of −30 kV. A dual channel plate detector is mounted on the end of the drift tube, and bias for the detector is supplied by a voltage divider between −30 kV and ground. The anode is at ground potential and is coupled to the digitizer through a 50 Ω feedthrough. This analyzer is limited to analysis of positive ions.

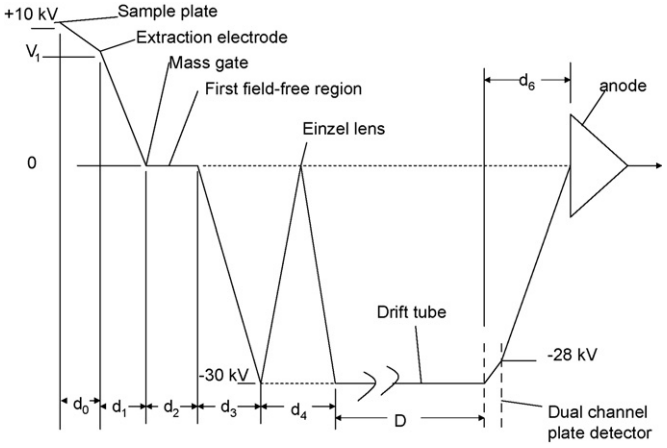

Fig. 3. Linear TOF mass analyzer with pulsed two-stage ion source at +10 kV and drift tube at −30 kV.

In this case the important limits are R_{s1}, R_{v1}, R_{Δ}, and R_{v2}, since second order velocity focusing with a linear analyzer, while possible, corresponds to impractical values of the parameters. If we increase the effective length of the source by decreasing the voltage pulse applied to the MALDI plate and increasing the bias voltage so that the total ion acceleration is constant, then the maximum resolving power at the focused mass can be increased as R_{s1} becomes smaller, but the resolving power decreases rapidly at masses other than the focused mass. This corresponds to increasing the value of the voltage ratio parameter $y = 40/(10 - V_1)$. The equations for the focal distances are modified slightly by the extra stages in the ion source accelerator. The total effective flight distance D_{e} corresponds to the length of a field-free region for which the flight time is identical to that through the actual system. For the system illustrated in Fig. 3 this is given by

$$D_{\mathrm{e}} = 2d_0 y^{1/2}\left[1 + \frac{d_1/d_0}{y^{1/2}+1}\right] + 2d_2 + \left(\frac{4}{3}\right)(d_3 + d_4) + D \tag{27}$$

The effective length for the space focus D_{s} relative to the exit from the pulsed acceleration is given by

$$D_{\mathrm{s}} = 2d_0 y^{3/2} \tag{28}$$

This is equivalent to Eq. (1) except that in the former equation the focus is relative to the entrance into the field-free drift space. The effective value of D_{v} is then given by Eq. (2). Calculation of effective and focusing distances and resolving power dependences are summarized in Table 1 as a function of voltage V_1 applied to the extraction plate. These calculation correspond to the analyzer configuration shown in Fig. 3 with distances $d_0 = 3$ mm, $d_1 = 3$ mm, $d_2 = 20$ mm, $d_3 = 12.5$ mm, $d_4 = 25$ mm, and $D = 1189$ mm. The uncertainties in initial position and initial velocity depend on the choice of MALDI matrix and may depend on the method used for preparing the sample. Under some conditions the estimated uncertainties are $\delta x = 0.01$ mm and $\delta v_0 = 0.0004$ mm/ns. The results summarized in Table 1 correspond to first order focus for 6 kDa.

The calculation of R_{Δ}^{-1} for $\delta_{\mathrm{j}} = 10$ ns in Eq. (6) corresponds to the value of the jitter between the laser pulse and the extrac-

Table 1
Calculated focal distances and resolving powers for linear analyzer focused at 6 kDa

V_1	y	D_e	D_s	$D_v - D_s$	Δt	R_{s1}^{-1}	R_{v1}^{-1}	R_t^{-1}	$\delta_j = 10$ ns		$\delta_j = 1$ ns	
									R_Δ^{-1}	$R(m^*)^{-1}$	R_Δ^{-1}	$R(m^*)^{-1}$
5	8	1300	136	1164	55	2,680	12,115	12,070	276	274	2,760	1,900
6	10	1302	190	1112	90	3,510	975	12,090	475	470	4,750	2,750
7	13.3	1305	292	1013	175	5,150	730	12,115	1010	988	10,100	4,290
8	20	1310	537	773	520	10,170	490	12,160	3950	3750	39,500	11,500

tion pulse determined experimentally. Clearly this is the major limitation on resolving power under essentially all conditions. Reducing this jitter to 1 ns substantially improves the resolving power and the value of the voltage ratio y can be chosen either to provide adequate resolving power over a broad mass range, e.g., $V_1 = 5$ kV, or higher resolving power at the focused mass but with a narrower range of focus with larger values of V_1. The contribution to the overall time resolution of the detector and digitizer is calculated for a 5 μm channel plate with a digitizer employing 0.5 ns bins, corresponding to a minimum peak width of about 1.5 ns.

The major effect due to an increase in the length of the analyzer is to decrease the contribution R_{v1} to the peak width, thus reducing the mass dependence of the resolving power. This is accompanied by a decrease in the effect of R_t on peak width, and large decrease in R_{v2}, but neither has a significant effect on overall resolving power. A longer drift tube length requires reducing the laser frequency inversely with the length for constant mass range, or decreasing the mass range inversely with the square of the drift tube length at constant laser frequency. With the geometry and voltages employed in this instrument the mass range is 0–180 kDa at a laser rate of 5 kHz. The overall conclusion is that there is little incentive for employing drift distances much greater than ca. 1 m in a linear analyzer. Also, a slower detector and wider digitizer bins can be used with the linear analyzer when the goal is nearly uniform resolving power over a wide mass range.

3. Summary of optimization strategy for reflecting analyzer

A two-stage ion source has the advantage that the focal length of the ion source can be varied by changing either the relative fraction of the total accelerating voltage applied in the first region of the ion source adjacent to the MALDI sample plate, the parameter y in the above equations, or by changing the delay time between the laser pulse and the high-voltage extraction pulse applied to the sample plate, Δt in Eq. (2). If the goal is to achieve maximum resolving power in an analyzer employing a reflector, then it is desirable to make the source as short as possible relative to the overall length and a single-field source is preferred as discussed below.

A potential diagram for a reflecting analyzer using a single-stage source and a two-stage reflector is shown in Fig. 2. In this diagram the length of the field-free space D is the total distance from source to mirror plus the distance from mirror to detector. With this analyzer adjusted for first and second order focusing the terms limiting the maximum resolving power are R_{s1}, R_{v3}, and R_t. The variation of resolving power with mass is determined primarily by R_{v1} and may also be affected by R_t. In terms of the dimensionless parameter $K = 2d_0/(D_v - D_s)$ the major contributions can be expressed as

$$R_{s1} = 2K^{-1}\left[\frac{\delta x}{D_e}\right] \tag{29}$$

$$R_{v3} = 4K^3\left(\frac{\delta v_0}{v_n}\right)^3 \tag{30}$$

and

$$R^2 = 4K^{-2}\left[\frac{\delta x}{D_e}\right]^2 + 16K^6\left(\frac{\delta v_0}{v_n}\right)^6 \tag{31}$$

The minimum value of R^2 corresponds to

$$-8K^{-3}\left[\frac{\delta x}{D_e}\right]^2 + 96K^5\left(\frac{\delta v_0}{v_n}\right)^6 = 0,$$

$$K^8 = \left(\frac{1}{12}\right)\left[\frac{\delta x}{D_e}\right]^2\left(\frac{\delta v_0}{v_n}\right)^{-6},$$

$$K = 0.733\left\{\frac{\delta x/D_e}{(\delta v_0/v_n)^3}\right\}^{1/4} \tag{32}$$

Replacing the ion velocity with the ratio of accelerating voltage to mass according to Eq. (5) gives the general expression:

$$K = 12^{-1/8}(D_e)^{-1/4}\{[\delta x {C_1}^3(\delta v_0)^{-3}\}^{1/4}\left(\frac{V}{m^*}\right)^{3/8} \tag{33}$$

The other major contributor to peak width is due to uncertainty in the time measurement due to the finite width of single ion pulses and the width of the bins in the digitizer. With standard 5 μm dual channel plate detectors and digitizers with 0.5 ns bins the uncertainty δt is about 1.5 ns. Commercial detectors are now available that provide single ion peak widths less than 0.5 ns and digitizers with 0.25 ns bins are available. These may allow the uncertainty, δt, in the time measurement to be reduced to about 0.75 ns. The limit on peak width is

$$R_t = \frac{\Delta m}{m} = \frac{2\delta t v_n}{D_e} = 2\left(\frac{\delta t}{D_e}\right)C_1\left(\frac{V}{m}\right)^{1/2} \tag{34}$$

The optimum value of V/m for given initial conditions and geometry can be determined by finding the minimum for R^2 due to

contributions from R_t and R_{v3}. Thus

$$R^2 = \left[\frac{2\delta t v_n}{D_e}\right]^2 + 16K^6\left(\frac{\delta v_0}{v_n}\right)^6 \quad (35)$$

The minimum value of R^2 corresponds to $d(R^2)/dv_n = 0$:

$$v_n = 12^{1/8}(K\delta v_0)^{3/4}\left(\frac{D_e}{\delta t}\right)^{1/4} = C_1\left(\frac{V}{m}\right)^{1/2} \quad (36)$$

The optimum value of K determined by optimizing between R_{s1} and R_{v3} is given by Eq. (32).

The overall optimum can be found by simultaneously satisfying both (32) and (36). This is satisfied for

$$v_n = \frac{\delta x}{K\delta t} \quad (37)$$

This condition corresponds to $R_{s1} = R_t$. The resulting peak width R is then given by

$$R = [2R_{s1}^2 + R_{v3}^2]^{1/2} \quad (38)$$

The global optimum conditions can be determined by substituting v_n as determined from Eq. (37) and determining the optimum value of K from the resulting equation. Thus from Eq. (31):

$$R^2 = 8K^{-2}\left[\frac{\delta x}{D_e}\right]^2 + 16K^6\left(\frac{\delta v_0}{v_n}\right)^6$$
$$= 8K^{-2}\left[\frac{\delta x}{D_e}\right]^2 + 16K^6(\delta v_0)^6\left(\frac{K\delta t}{\delta x}\right)^6 \quad (39)$$

And the minimum value found for $d(R^2)/dK = 0$ is

$$K = (12)^{-1/14}\left(\frac{\delta x}{\delta t \delta v_0}\right)^{3/7}\left(\frac{\delta x}{D_e}\right)^{1/7} \quad (40)$$

The optimum value of V/m is given by

$$\frac{V}{m} = \left(\frac{\delta x}{KC_1\delta t}\right)^2 \quad (41)$$

Eqs. (40) and (41) give the focusing parameter K and voltage V corresponding to maximum resolving power for a given mass m with an analyzer of effective length D_e, for time measurement uncertainty δt, initial velocity spread δv_0, and initial position uncertainty δx.

The major contributions to peak width at optimal V/m are summarized for some typical parameter values as functions of K in Fig. 4. The plotted curves correspond to

$$R_{st} = (R_{s1}^2 + R_t)^{1/2} = 2^{1/2}R_{s1} = 8^{1/2}K^{-1}\left(\frac{\delta x}{D_e}\right) \quad (42)$$

and

$$R_{v3} = 4K^6\left(\frac{\delta v_0 \delta t}{\delta x}\right)^3 \quad (43)$$

The plots shown in Fig. 4 correspond to $\delta t = 0.75$ ns, $\delta x = 0.01$ mm, for $D_e = 3.2$ and 12.8 m and $\delta v_0 = 400$ and 800 m/s. Eqs. (41)–(43) allow the optimal operating conditions to be determined by for any specified initial conditions and analyzer geometry. Optimum values of K and V/m as functions of effective length are shown in Figs. 5 and 6 for one set of initial conditions and values of $\delta t = 0.75$ and 1.5 ns. Calculated maximum resolving power as function of effective length is shown in Fig. 7 over the range from 0.4 to 6.4 m, and over the extended range to

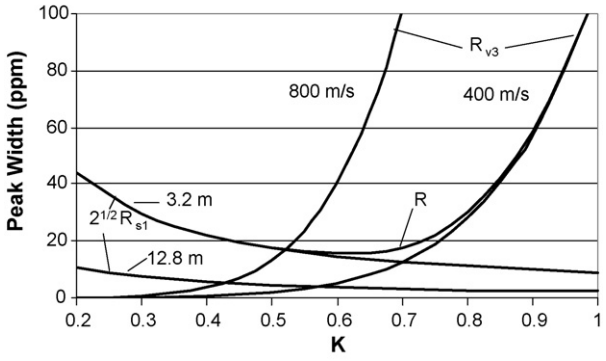

Fig. 4. Calculated contributions to peak width for reflecting analyzer as function of $K = 2d_0/(D_v - D_s)$, at optimum value of V/m so that $R_{s1} = R_t$.

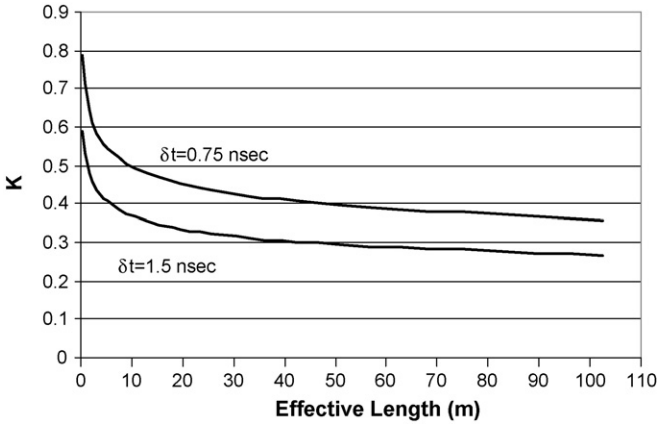

Fig. 5. Optimum value of $K = 2d_0/(D_v - D_s)$ for $\delta v_0 = 400$ m/s and $\delta x = 10$ μm as function of effective length of analyzer in meters.

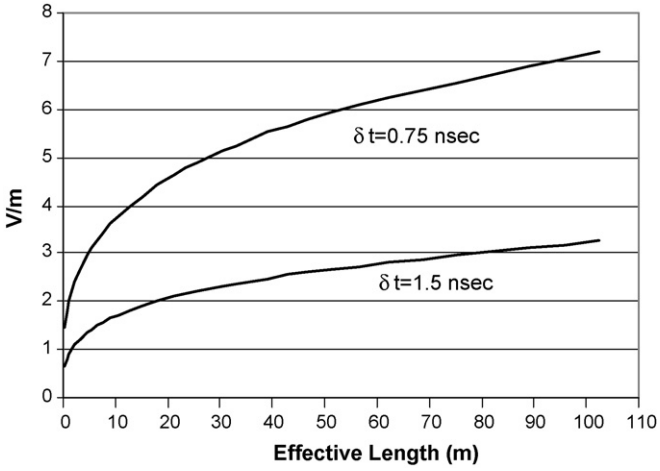

Fig. 6. Optimum V/m for $\delta v_0 = 400$ m/s and $\delta x = 10$ μm as function of effective length of analyzer in meters.

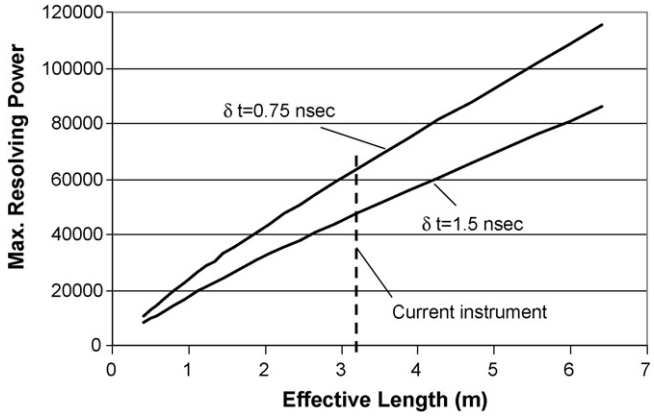

Fig. 7. Calculated maximum resolving power for optimized reflecting analyzer for $\delta v_0 = 400$ m/s and $\delta x = 10$ μm as function of effective length of analyzer in meters over the range from 0.4 to 6.4 m. Parameter δt is the peak width for single ions as determined by the uncertainty in the time measurement.

102.8 m in Fig. 8. The vertical dashed line in Fig. 7 corresponds to the analyzer with $D_e = 3200$ mm used for initial validation of the theory. The optimum values are then $K = 0.46$ and $V/m = 1.1$ for $\delta t = 1.5$ ns.

Increasing the length by a factor of 2 provides improvement in resolving power by about a factor of 1.8. Other possible contributions such as R_L should also be proportional to D_e^{-1}. R_V is independent of length and very low noise high voltage supplies are required to achieve the very high resolving power theoretically possible using a longer analyzer. The overall length of the analyzer is approximately equal to $0.4D_e$, thus achieving a resolving power of 1,000,000 requires an analyzer about 40 m in length. The cost of increasing the length is minimal since only a longer flight tube and mirror are required; all other elements are unchanged. The practical limitation is the size of the laboratory.

Increasing the length of the analyzer also improves the breadth of focus. Calculated resolving powers as a function of m/z can be used to independently asses the contribution due to velocity spread and uncertainty in initial position. The contribution to peak width due to mass dependence of the first order

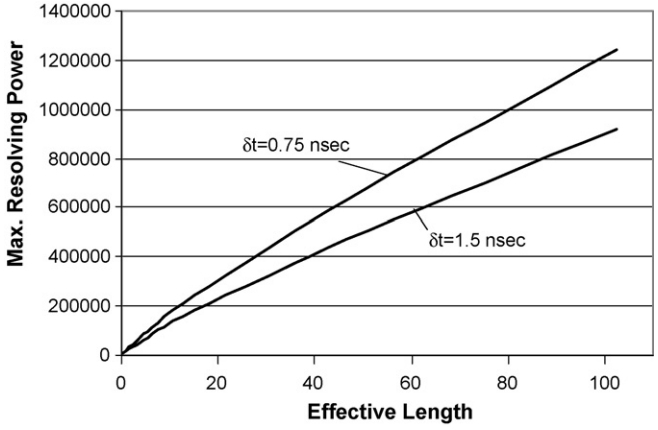

Fig. 8. Calculated maximum resolving power for optimized reflecting analyzer for $\delta v_0 = 400$ m/s and $\delta x = 10$ μm as function of effective length of analyzer in meters over the range from 0.4 to 102 m. Parameter δt is the peak width for single ions as determined by the uncertainty in the time measurement.

focus is given by

$$R_m = R_{v1}\left[1 - \left(\frac{m}{m^*}\right)^{1/2}\right]$$

where

$$R_{v1} = \left(\frac{4d_0}{D_e}\right)\left(\frac{\delta v_0}{v_n}\right) = \left(\frac{4d_0}{D_e}\right) K \left(\frac{\delta v_0 \delta t}{\delta x}\right) \quad (44)$$

This becomes the dominant factor determining peak width for masses significantly different from the focus mass. This factor is directly proportional to the source length d_0, and suggests that this should be made as short as possible with the ultimate limit being set by conditions for electrical discharge in the source.

The contribution to peak width due to jitter between the laser pulse and the extraction pulse is

$$R_\Delta = 2\left(\frac{\delta_j \delta v_0}{D_e}\right)\left[\frac{D_v - D_s}{2d_0}\right]^2 = (2K^{-2})\left(\frac{\delta_j \delta v_0}{D_e}\right) \quad (45)$$

Using typical values discussed above, $\delta_j = 10$ ns, $\delta v_0 = 0.0004$ mm/ns, $K = 0.5$ the resolving power limit due to this effect is $31D_e$ or about 100,000 with an analyzer of 3200 mm effective length. Thus, unlike the linear analyzer a jitter of 10 ns between laser pulse and extraction pulse is insignificant.

4. Experimental results

An example of a spectrum from a calibration mixture containing bovine insulin (5736), e-coli thioredoxin (11,675) and equine apomyoglobin (16,952) obtained with the linear analyzer is shown in Fig. 9. The matrix was sinipinic acid and 1 μL of solution containing 50 fmol insulin, 300 fmol thioredoxin, and 400 fmole myoglobin was deposited on 1.5 mm spots on the sample plate. Most of the peaks in the spectrum can be accounted for by singly protonated monomers and dimers, matrix adducts, and multiply protonated monomers and dimers. Some additional peaks appear to be fragments of the higher molecular weight proteins, possibly formed in the first field-free region. Inset A shows an expansion of the molecular ion region for myoglobin, and inset B is the same region obtained with about 10% less laser power. Experimental resolving power for several peaks in each spectrum are compared with a theoretical calculation in Fig. 10.

A spectrum of a tryptic digest of BSA taken with the reflecting analyzer is shown in Fig. 11. These results were obtained with an ion energy of 8 kV corresponding according to the theory to conditions for an optimum focus mass of about 7 kDa. For lower masses the resolving power can be improved by reducing the ion energy. Experimental resolving power at 1567 is about 15,000 and is greater than 12,000 over the range shown. The external calibration was corrected using single-point internal calibration on the matrix trimer. Nine peptides with intensity greater than 5% of the base peak correspond to fully tryptic fragments of BSA with deviations between theoretical and experimental masses of less than 10 ppm. RMS error is 4.5 ppm for these peptides. An additional eight peptides with intensities between 1 and 5% of the base peak also correspond to BSA peptides

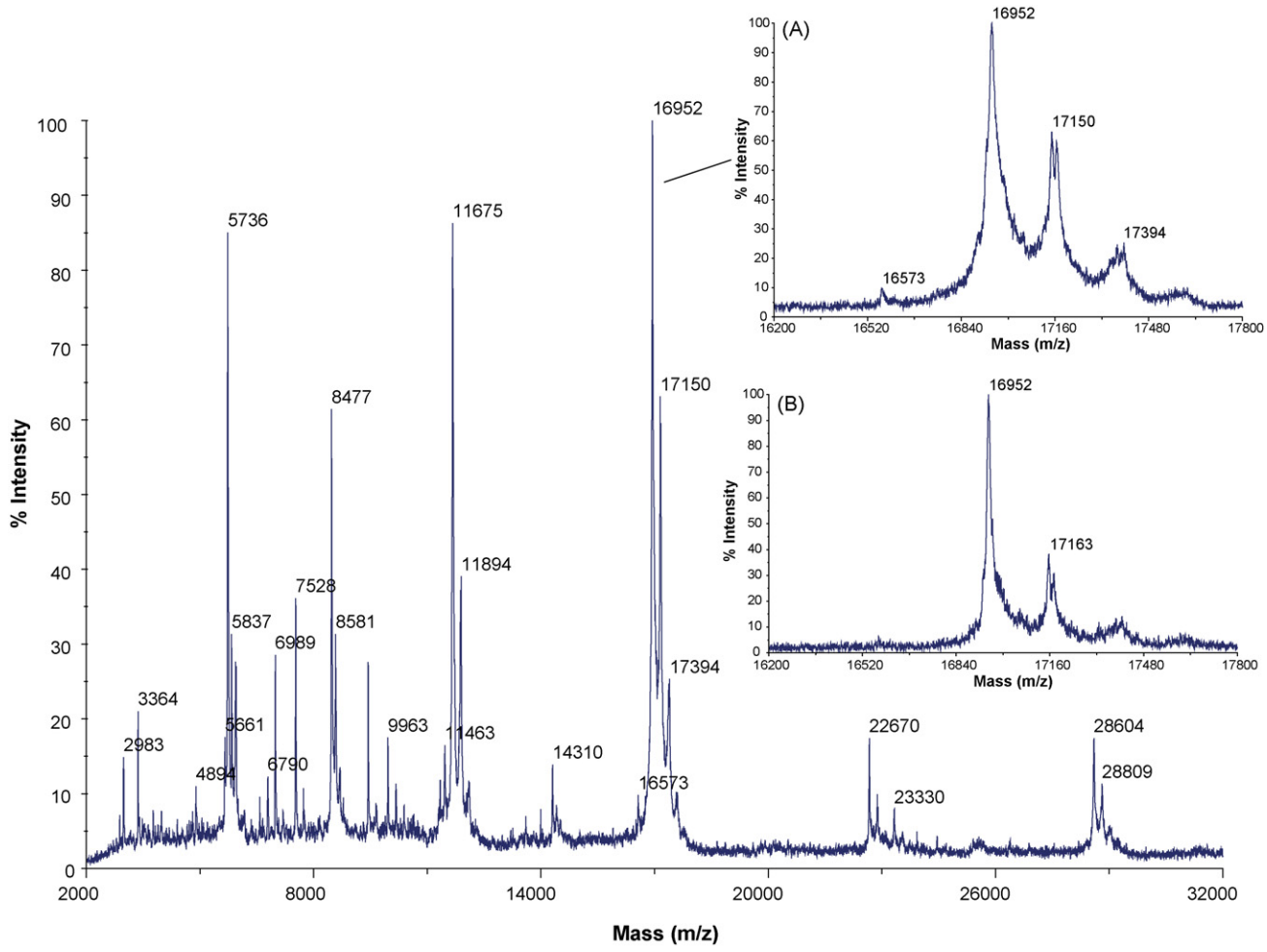

Fig. 9. Spectra of proteins measured with linear analyzer focused to provide adequate resolving power over a broad range of masses. $V_1 = 7$ kV, $\Delta t = 320$ ns, $\delta t = 4$ ns, and $\delta_j = 10$ ns. Sample is mixture of bovine insulin, e-coli thioredoxin, and equine myoglobin in sinipinic acid matrix. Inset (A) shows the molecular ion region of myoglobin at high laser power and (B) shows the same region from another spectrum taken at ca. 10% lower laser power.

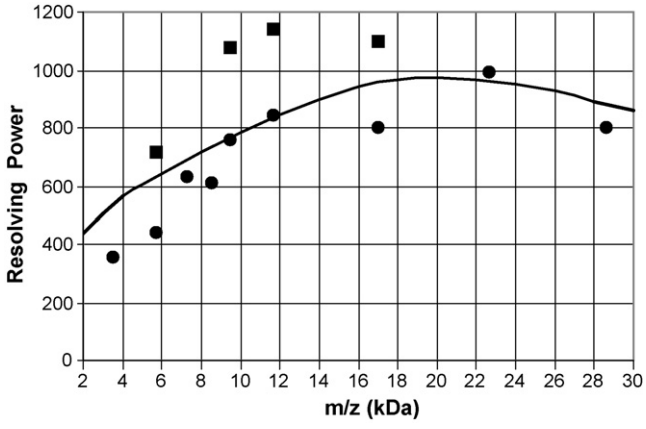

Fig. 10. Comparison of calculated resolving power (line) as function of m/z for linear analyzer focused at 20 kDa compared with experimental results, circle at high laser power, square at low laser power from data for mixture of bovine insulin, e-coli thioredoxin, and equine myoglobin.

within the same error limits. Four other peaks in this intensity range also correspond to BSA tryptic peptides, but the errors for these are in the range of 10–20 ppm. One of these (1749) is clearly due to an unresolved doublet with the second isotope peak of 1747, and the other three are at higher mass where there appears to be a systematic error in the calibration. The observed peaks account for about 40% coverage of the BSA sequence.

The maximum resolving power observed in the reflector is more than a factor of two lower than calculated. Possible sources of this discrepancy are either trajectory error due to misalignment between the mirror and the detector resulting from improper alignment of the drift tube flanges or noise on the high voltages applied to the ion mirror. As indicated by Eq. (23) an angular error of ca. 0.3° can account for the problem. A new drift tube was fabricated and the system carefully realigned with no detectable improvement in resolving power. Filters were added on the output of the high voltage power supplies that reduced the amplitude of the ripple (65 kHz) by more than an order of magnitude with no detectable improvement in resolving power. Subsequent measurement of low frequency noise (less than 60 Hz) showed about 2 V of noise in this frequency range

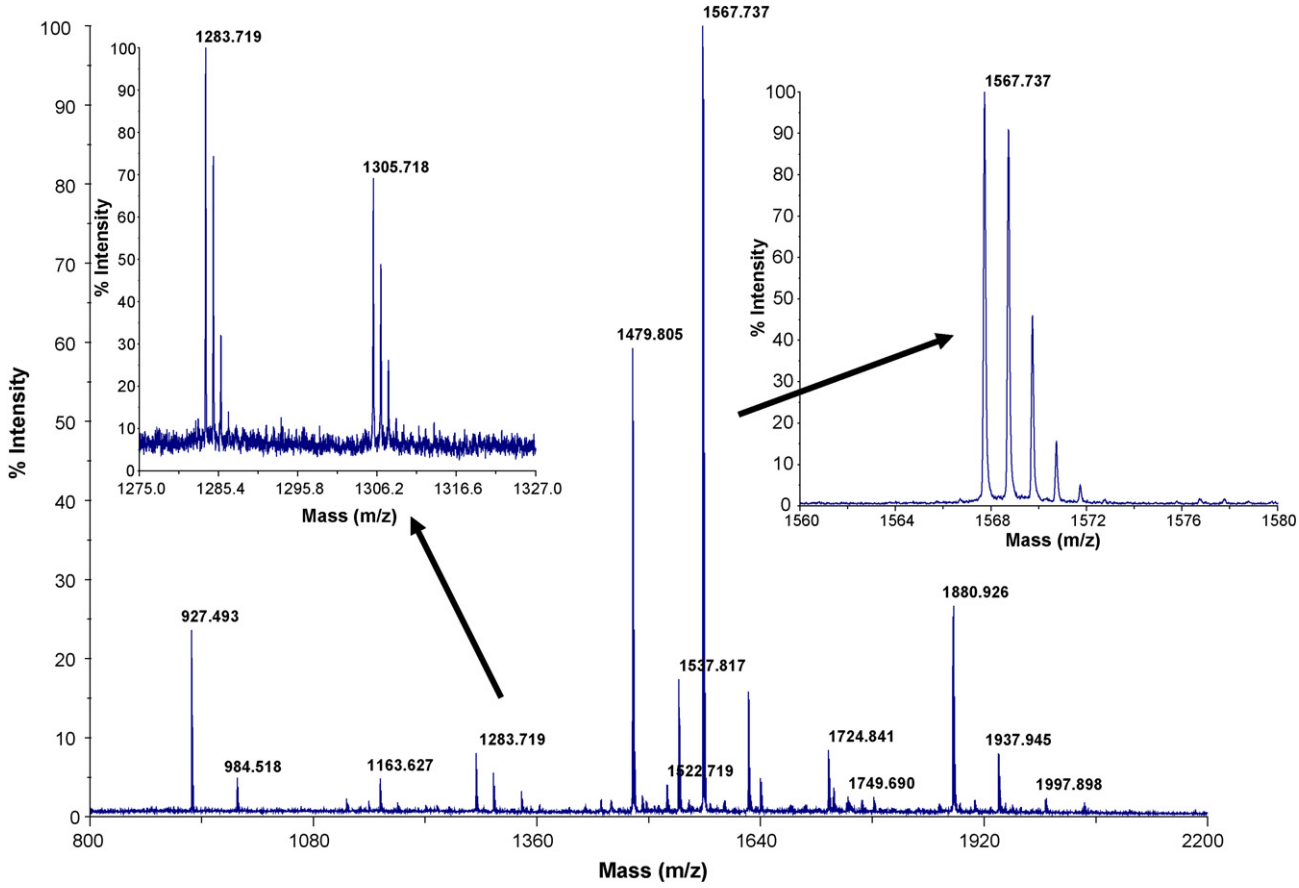

Fig. 11. Spectrum of tryptic digest of BSA measured with the optimized reflecting analyzer. $\delta t = 1.5$ ns and $\delta_j = 10$ ns.

that appears to be the major factor limiting the resolving power. Specification of noise in this low frequency range is not normally included in the specifications supplied by the power supply manufacturers. Power supplies with ripple, low frequency noise, and load regulation better than 2 ppm have been ordered recently, and barring other hidden limits on peak width these changes should make it possible to approach the theoretical resolving power.

5. Summary

Some work remains to demonstrate that the resolving power predicted for an optimized analyzer according to the theory described can be realized in practice. Some useful conclusions include the following:

(1) The resolving power of the optimized reflecting analyzer is nearly proportional to the effective length of the analyzer, but is almost independent of the effective length for a linear analyzer.
(2) Jitter between the laser pulse and the extraction pulse is often the most important limit on resolving power for a linear analyzer, but is relatively unimportant for a reflector.
(3) In a reflecting analyzer the ion source should be made as short as possible without introducing electrical discharge in the ion source.
(4) The ion energy should be as high as practical for a linear analyzer for application to proteins, but best resolving power for a reflecting analyzer for peptides requires lower energy than is typically used.
(5) The ultimate resolving power of a reflecting analyzer is proportional to the square root of the uncertainty in the time measurement, but resolving power of a linear analyzer is not strongly dependent on the time measurement uncertainty.
(6) The practical upper limit on the resolving power of a reflecting analyzer is determined by the size of the laboratory and noise on the high voltage supplies.

This initial optimization has focused on resolving power rather than sensitivity. In general higher resolving power provides higher sensitivity since the peaks are higher and narrower, and this improves the ability to detect and identify peptides in the presence of chemical noise. On the other hand, reducing the ion energy to increase resolving power may lead to a reduction in the efficiency of ion transmission and detection. The use of faster detectors and improved digitizers ultimately allows higher values of V/m leading either to improved resolving power at low mass or higher optimal values of V to improve ion transmission and detection. Future work will focus on global optimization of resolving power, sensitivity, and dynamic range, and on extending to higher laser rates to optimize the combination of speed and sample utilization.

References

[1] M. Karas, F. Hillenkamp, Anal. Chem. 60 (1988) 2299.
[2] J. Fenn, M. Mann, C.K. Meng, S.F. Wong, Science 246 (1989) 64.
[3] M.L. Vestal, P. Juhasz, J. Am. Soc. Mass. Spectrom. 9 (1998) 892.
[4] M.L. Vestal, P. Juhasz, S.A. Martin, Rapid Commun. Mass Spectrom. 9 (1995) 1044.
[5] W.C. Wiley, I.H. McLaren, Rev. Sci. Instrum. 26 (1955) 1150.
[6] B.A. Mamyrin, V.I. Karataev, D.V. Shmikk, V.A. Zagulin, Sov. Phys. JETP 37 (1973) 45.